ATTACHMENT

CONSUMERS ENERGY COMPANY
PALISADES PLANT
DOCKET 50-255

# Consumers Energy (Westinghouse) Reactor Vessel Neutron Fluence Methodology

Table of Contents

# 1.0 Westinghouse Reactor Vessel Neutron Fluence Methodology

The methodology used by Westinghouse to perform neutron exposure evaluations of Light Water Reactor (LWR) pressure vessels is designed to provide "best estimate" exposure projections in terms of fast neutron fluence [$\Phi$(E > 1.0 MeV)] and iron atom displacements [dpa]. The methodology is also intended to provide uncertainty estimates associated with these "best estimate" exposure projections.

The use of "best estimate" values for $\Phi$(E > 1.0 MeV) and dpa in the assessment of pressure vessel embrittlement is consistent with the requirements of 10 CFR 50.61, "Fracture Toughness Requirements for Protection Against Pressurized Thermal Shock Events."[1] In 10 CFR 50.61, evaluation of the reference temperature [$RT_{PTS}$] is required to be performed using "best estimate" values of neutron exposure and material properties. Uncertainty in the $RT_{PTS}$ determination (e.g., from uncertainty in the neutron exposure, chemistry factor, or shift correlation) is treated separately by adding an explicit margin term to the calculated value. The use of "best estimate" values for $\Phi$(E > 1.0 MeV) and dpa is also promulgated in Draft Regulatory Guide DG-1053, "Calculational and Dosimetry methods for Determining Pressure Vessel Neutron Fluence."[2]

For the purposes of the following discussion, the "best estimate" is defined as a neutron exposure in terms of $\Phi$(E > 1.0 MeV) and dpa resulting from a combination of plant specific neutron transport calculations and available measurement data to produce an accurate assessment of the pressure vessel exposure while minimizing the uncertainty associated with the assessment. The general philosophy supporting this definition is that, in order to minimize the uncertainties associated with the reactor vessel exposure projections, plant specific neutron transport calculations must be supported by benchmarking the analytical approach and by combination with measurements.

The analytical benchmarking and measurement comparisons are carried out in the following three stages:

1. Comparisons with benchmark measurements from the PCA simulator at ORNL[3] and the Standard U-235 spectrum field. This phase of the methods qualification addresses the adequacy of basic transport calculation and dosimetry evaluation techniques and cross-sections, but does not test the accuracy of core neutron source calculations nor does it address uncertainties in operational and geometric variables that impact power reactor calculations.
2. Comparisons with power reactor benchmarks such as H. B. Robinson 2[4] and other industry wide dosimetry data bases. This phase of the testing addresses biases and uncertainties that are primarily methods related and would tend to apply generically to all fast neutron exposure evaluations.
3. Comparisons with plant specific measurements. This final stage of the process acts to identify uncertainties and biases that may vary from plant to plant. This would include effects of actual vs. nominal reactor dimensions, actual vs. nominal system temperatures, and the impact of using time averaged variables such as power distribution shape and magnitude in the transport calculations.

This benchmarking approach establishes a progression from a purely analytical approach tied to experimental benchmarks to an approach that makes use of industry and plant specific power reactor measurements to remove potential generic and plant specific biases in the analytical method. Therefore, knowledge regarding the neutron environment applicable to a specific reactor vessel is increased and the uncertainty associated with vessel exposure projections is minimized, resulting in an overall "best estimate" neutron exposure evaluation.

## 2.0 Historical Perspective of the Neutron Fluence Methodology

The analytical and measurement evaluation techniques employed by Westinghouse to determine the best estimate pressure vessel fluence have evolved over time to the current NRC-approved method described in WCAP-14040-NP-A.[5] In particular, the best estimate vessel exposure is obtained from the following relationship:

$$\Phi_{Best\ Est.} = K\ \Phi_{Calc.} \qquad \text{Eq. 2-1}$$

where:

$\Phi_{Best.\ Est.}$ = The best estimate fast neutron exposure at the location of interest; i.e, at the pressure vessel wall.

K = The plant specific measurement/calculation (M/C) bias factor derived from all available surveillance capsule and reactor cavity dosimetry data.

$\Phi_{Calc.}$ = The absolute calculated fast neutron exposure at the location of interest.

This evolution was promulgated primarily by advances in computer technology, allowing for more detailed analyses at reduced costs. These advances highlighted deficiencies in the nuclear data input to the analytical models and lead to re-evaluations and updates to these data libraries.

Prior to the mid-70's the reactor vessel neutron fluence was calculated using one-dimensional multigroup diffusion employing the P1MG code[6] or one-dimensional discrete ordinates transport employing ANISN[7] and no explicit modeling of the surveillance capsules. A typical core source was input to the calculation to obtain a 1-D relative neutron spectrum. This calculated relative spectrum at the capsule location was then combined with reaction specific spectrum average cross-sections and normalized to the measurements to determine the capsule exposure $\phi(E > 1.0\ MeV)$. The reactor vessel neutron fluence was then determined by applying a standard lead factor to the measured capsule fluence and projecting to the end-of-life.

Between mid-70's and early 80's the reactor vessel neutron fluence was calculated using two-dimensional discrete ordinates transport employing the DOT code.[8] The use of 2-D calculations allowed for explicit modeling of the capsule. From a neutronic standpoint, the surveillance capsules and associated support structures are significant. The presence of these materials has a marked effect on both the spatial distribution of neutron flux and the neutron energy spectrum in the water annulus between the core barrel or

thermal shield and the reactor vessel. Additionally, ENDF/B-II based transport cross-sections[9] were available and used in the calculations.

A reference, design-basis, spatial core power distribution was used to calculate the neutron exposure at the capsule and pressure vessel. The capsule exposure $\phi$(E > 1.0 MeV) was then determined using the reaction specific spectrum average cross-sections and measurements. The reactor vessel neutron fluence was then determined by applying an analytically determined lead factor to the measured capsule fluence and projecting to the end-of-life. The transition to a 2-D analytical model to determine the spectrum average cross-sections greatly improved the consistency of the measured fluence determined from the different reactions, i.e. $^{54}$Fe (n,p), $^{58}$Ni (n,p), $^{238}$U (n,f), and $^{237}$Np (n,f).[10]

Through this time period the reaction rates referenced to full power were determined using the measured activities decay corrected to the cycle shutdown. The neutron transport methodology employed a generic, design basis core source distribution, in which cycle-to-cycle flux variations were not considered. Thus the reaction rate was derived as:

$$R = \frac{A}{N_o F Y \sum_{j=1}^{n} \frac{P_j}{P_{max}} (1 - e^{-\lambda t_j}) e^{\lambda t_d}}$$

Eq. 2-2

where,

| | | |
|---|---|---|
| R | = | reaction rate averaged over the irradiation period and referenced to operation at a core power level of $P_{ref}$ (rps/nucleus) |
| A | = | measured specific activity (dps/g) |
| $N_o$ | = | number of target element atoms per gram of sensor |
| F | = | weight fraction of the target isotope in the sensor material |
| Y | = | number of product atoms produced per reaction |
| $P_j$ | = | average core power level during irradiation period j |
| $P_{max}$ | = | maximum or reference core power level |
| $\lambda$ | = | decay constant of product nuclide |
| $t_j$ | = | length of irradiation period j |
| $t_d$ | = | decay time following irradiation period j |
| n | = | total number of irradiation periods |

With the release of the ENDF/B-IV based transport cross-sections in the SAILOR library[11], the measured fluence at the capsule changed due to the ENDF/B-IV based spectrum average cross-sections. However, the reactor vessel neutron fluence was still determined by applying an analytically determined lead factor to the measured capsule fluence and projecting to the end-of-life.

Around the early to mid 80's Westinghouse adopted a least squares analysis technique, the FERRET code[12], to determine the best estimate fluence at the capsule and pressure vessel. The least squares analysis technique was well established within the industry as documented in ASTM E944[13]. Additionally, the FERRET least squares analysis code had been used as part of the LWR Pressure Vessel Surveillance Dosimetry Improvement Program via the PCA & PSF benchmarks and the H.B. Robinson 2 Cycle 9

experiment.

Two-dimensional calculations were transitioned to using the DORT code[14] with the ENDF/B-IV based SAILOR library transport cross-sections. Additionally, plant specific spatial core power distributions were used due to the plants modifying the core management and changing from out-in fuel loading to low-leakage loading patterns. The low-leakage patterns placed once-, twice-, and thrice burned assemblies at the periphery, rather than fresh fuel assemblies, to reduce the neutron flux on the vessel. The best estimate neutron fluence at the pressure vessel was then determined by Equation 2.1.

In 1994, the ENDF/B-VI based transport cross-sections were released in the BUGLE-93 library[15]. The underpredictions of the calculated fluence that were widely observed using the SAILOR library due to the treatment of the $^{56}Fe$ inelastic scattering cross-section showed significantly improved agreement with the measured data with the release of BUGLE-93. The Westinghouse methodology for calculating the best estimate pressure vessel fluence continues to be described by Equation 2.1.

From about the time of release of the ENDF/B-IV based cross-section libraries, the analytical neutron fluxes were determined using plant-specific spatial core power distributions, as described above. As plants began to change core management by moving from an out-in fuel loading pattern to low-leakage or in-out patterns, cycle-to-cycle flux variations became apparent. The methodology for calculating the reaction rates evolved to account for changes in sensor reaction rates caused by variations in flux level induced by changes in the core spatial power distributions from cycle to cycle. Thus the reaction rate was derived as:

$$R = \frac{A}{N_o F Y \sum_{j=1}^{n} \frac{P_j}{P_{max}} C_j (1 - e^{-\lambda t_j}) e^{\lambda t_d}}$$

Eq. 2-3

where,

$C_j$ = Calculated ratio of $\phi(E > 1.0\ MeV)$ during irradiation period j to the time weighted average $\phi(E > 1.0\ MeV)$ over the entire irradiation period

Table 2-1 provides a summary of the evolution of the methodology. It is important to recognize that the measurements, i.e. the measured specific activities (A in Equations 2-2 and 2-3), have not changed, just the calculational methodology.

Table 2-1

Evolution of the Westinghouse Reactor Vessel Neutron Fluence Methodology

| Calculational Methods | Reaction Rates | Fluence |
|---|---|---|
| **Prior to the mid-70's** | | |
| 1-D spectrum via P1MG diffusion or ANISN discrete ordinates methods, representative core power distributions, No capsule model in transport calculation, Spectrum average cross-sections. | $R=\frac{A}{N_o FY\sum_{j=1}^{n}\frac{P_j}{P_{max}}(1-e^{-\lambda t_j})e^{\lambda t_d}}$ | $\Phi=\frac{R}{\bar{\sigma}}t_j$ |
| **Mid-70's to early 80's** | | |
| 2-D spectrum via DOT discrete ordinates methods employing ENDF/B-II cross-sections, Design basis core power distributions, Capsule model in transport calculation, Spectrum average cross-sections. | $R=\frac{A}{N_o FY\sum_{j=1}^{n}\frac{P_j}{P_{max}}(1-e^{-\lambda t_j})e^{\lambda t_d}}$ | $\Phi=\frac{R}{\bar{\sigma}_1}t_j$ |
| **Early 80's** | | |
| 2-D spectrum via DOT discrete ordinates methods employing ENDF/B-IV cross-sections, Plant specific core power distributions, Capsule model in transport calculation, Spectrum average cross-sections. | $R=\frac{A}{N_o FY\sum_{j=1}^{n}\frac{P_j}{P_{max}}C_j(1-e^{-\lambda t_j})e^{\lambda t_d}}$ | $\Phi=\frac{R}{\bar{\sigma}_2}t_j$ |
| **Early/mid-80's to 1994** | | |
| 2-D spectrum via DOT/DORT discrete ordinates methods employing ENDF/B-IV cross-sections, Plant specific core power distributions, Capsule model in transport calculation, Least squares evaluation of calculations and measurements to determine best estimate fluence. | $R=\frac{A}{N_o FY\sum_{j=1}^{n}\frac{P_j}{P_{max}}C_j(1-e^{-\lambda t_j})e^{\lambda t_d}}$ | $\Phi_{BE}$ |
| **1994 to present** | | |
| 2-D spectrum via DORT discrete ordinates methods employing ENDF/B-VI cross-sections, Plant specific core power distributions, Capsule model in transport calculation, Least squares evaluation of calculations and measurements to determine best estimate fluence. | $R=\frac{A}{N_o FY\sum_{j=1}^{n}\frac{P_j}{P_{max}}C_j(1-e^{-\lambda t_j})e^{\lambda t_d}}$ | $\Phi_{BE}$ |

# 3.0 Methodology Benchmarking

## *3.1 $S_n$ Transport Calculations*

### 3.1.1 Comparisons with the PCA Pressure Vessel Simulator Benchmark

The pressure vessel simulator benchmark comparisons used in the qualification of the neutron transport methodology are based on the analysis of the PCA 12/13 experimental configuration.[3,16,17] A schematic description of this configuration is provided in Figures 3.1.1-1 and 3.1.1-2. A plan view of the PCA reactor and pressure vessel simulator showing materials characteristic of the core axial midplane is shown in Figure 3.1.1-1; whereas, a section view through the center of the mockup is shown in Figure 3.1.1-2. The description of the 12/13 configuration was derived from information provided in References 3, 16, and 17 and reflects the latest available geometric data for the simulator.

The 12/13 configuration was chosen for the methods evaluation due to the similarity of this particular mockup to the thermal shield - downcomer - pressure vessel designs that are typical of most pressurized water reactors. Of particular note in regard to the areas of similarity are the 12 cm water gap on the core side of the thermal shield, the 13 cm water gap between the thermal shield and the pressure vessel simulator, the 6 cm thick thermal shield, the 22.5 cm thick low alloy steel pressure vessel, and the simulated reactor cavity (void box) positioned behind the pressure vessel mockup.

From the viewpoint of fast neutron attenuation, the 12/13 experimental configuration results in a reduction factor for $\phi(E > 1.0\ MeV)$ of approximately 1000 between the reactor core and the inner surface of the pressure vessel; and a corresponding reduction factor of about 30 from the inner surface to the outer surface of the pressure vessel wall. These similarities in the geometry and attenuation properties of the PCA mockup and LWR plant configurations provide additional confidence that judgments made regarding measurement/calculation comparisons in the simulator environment can be related to the subsequent analyses performed for operating Light Water Reactors.

During the PCA experiments, measurements were obtained at several locations within the mockup to provide traverse data extending from the reactor core outward through the pressure vessel simulator and on into the void box. The specific measurement locations are illustrated on Figure 3.1.1-1 and listed in Table 3.1.1-1. From Figure 3.1.1-1 it is noted that all of the measurements were obtained on the lateral centerline of the mockup. Furthermore, all of the measurement points were also positioned on the axial midplane of the simulator.

Figure 3.1.1-1
PCA 12/13 Configuration - X,Y Geometry

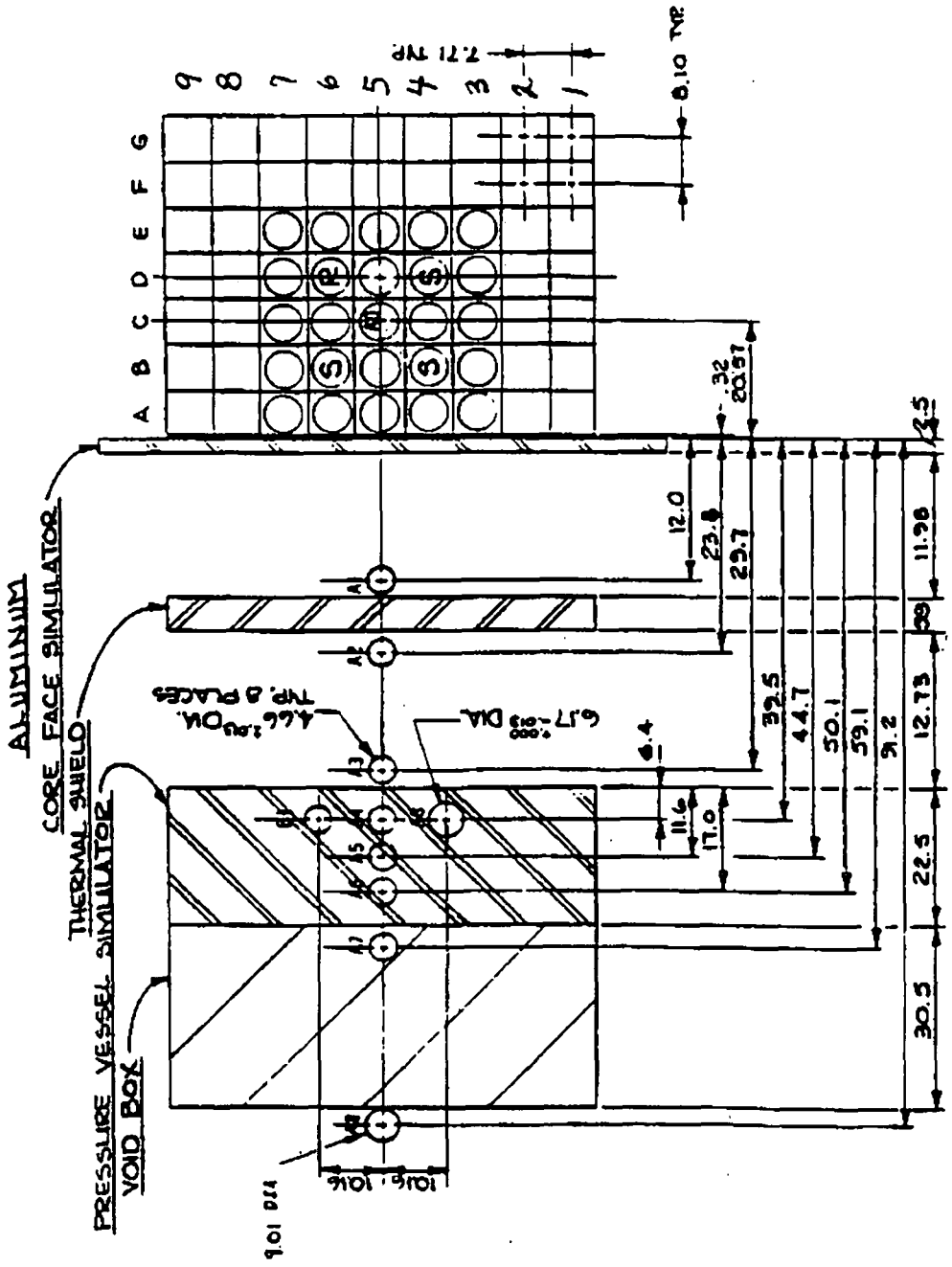

Figure 3.1.1-2
PCA 12/13 Configuration - Y,Z Geometry

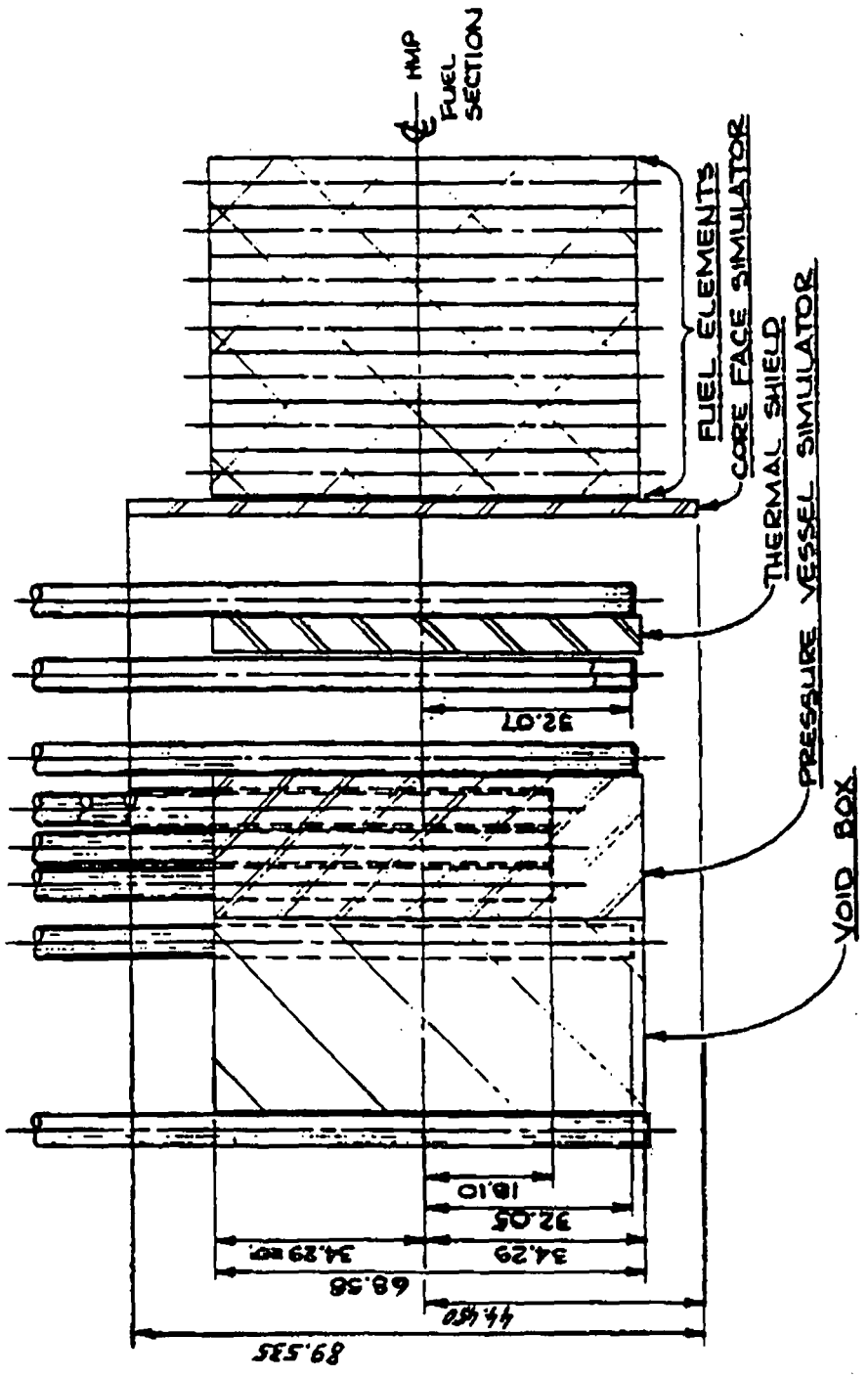

Table 3.1.1-1
Summary Of Measurement Locations Within The PCA 12/13 Configuration

| Location | ID | Y (cm) |
|---|---|---|
| Core Center | A0 | -20.75 |
| Thermal Shield Front | A1 | 11.98 |
| Thermal Shield Back | A2 | 22.80 |
| Pressure Vessel Front | A3 | 29.71 |
| Pressure Vessel ¼T | A4 | 39.51 |
| Pressure Vessel ½T | A5 | 44.67 |
| Pressure Vessel ¾T | A6 | 50.13 |
| Void Box | A7 | 59.13 |

Note: Y dimensions are referenced to the core side face of the aluminum window (see Figure 3.1.1-1).

The measurement locations specified in Table 3.1.1-1 provide data sufficient to generate measurement/calculation comparisons throughout the entire 12/13 configuration. Data from locations A4, A5, and A6 establish the means for verification of calculated exposure gradients within the pressure vessel wall itself. Since measurements at operating power reactors can, at best, provide data in the downcomer region internal to the vessel wall or in the cavity external to the vessel wall, these PCA data points located interior to the thick walled vessel establish a key set of comparisons to aid in the accurate determination of exposure gradients within the pressure vessel wall.

Method of Analysis

The initial neutron transport analysis of the PCA 12/13 configuration was carried out using two DORT two-dimensional discrete ordinates transport calculations, one in X,Y geometry and one in Y,Z geometry, as well as a single one-dimensional DORT calculation in planar (Y) geometry to synthesize a three-dimensional solution throughout the PCA simulator. The synthesis was carried out using the following relationship:

$$\phi_g(x,y,z) = \phi_g(x,y) * \frac{\phi_g(y,z)}{\phi_g(y)} \qquad \text{Eq. 3-1}$$

where:

$\phi_g(x,y,z)$ = The group-g neutron flux at position x,y,z within the problem geometry.
$\phi_g(x,y)$ = The group-g neutron flux solution from the x,y DORT computation.
$\phi_g(y,z)$ = The group-g neutron flux solution from the y,z DORT computation.
$\phi_g(y)$ = The group-g neutron flux solution from the y DORT computation.

In this synthesis approach the ratio $[\phi_g(y,z)]/[\phi_g(y)]$ represents an energy dependent axial shape factor that accounts for the finite height of the PCA core as well as for axial leakage effects introduced by the simulator geometry.

In the calculation of the PCA 12/13 configuration, all of the DORT computations were carried out in 67 energy groups (47 neutron, 20 gamma-ray) using a $P_3$ cross-section expansion from the BUGLE-93 transport cross-section library and an $S_8$ order of angular quadrature. The geometric models used in the

calculations consisted of 71×131, 131×71, and 131 mesh cell arrays for the X,Y, Y,Z, and Y problems, respectively. Material descriptions for each of the regions comprising the simulator geometry were taken as specified in References 3, 16, and 17. Likewise, the spatial distribution of the neutron source within the PCA core was obtained directly from References 3, 16, and 17. In generating the energy dependent source for use in the transport calculations, the specified spatial distribution was coupled with the ENDF/B-VI $^{235}U$ fission spectrum supplied with the BUGLE-93 library. Dosimeter reaction rates for comparison with PCA measurements were derived from the synthesized three-dimensional neutron flux distribution using the ENDF/B-VI reaction cross-sections also supplied with the BUGLE-93 library.

Comparison of PCA Calculations with Measurements

Measured data from the PCA experiments using the 12/13 simulator configuration have been documented and discussed extensively in References 3, 16, and 17. In these documents, individual sensor measurements were provided in terms of either equivalent fission flux per source neutron or absolute reaction rates per source neutron for a variety of reactions with responses spanning the fast neutron energy range. For the comparisons presented in this report all equivalent fission fluxes were converted to absolute reaction rates using fission spectrum averaged reaction cross-sections that were also reported in the PCA documentation. In particular, the following reaction cross-sections were employed to perform the required conversions:

| Reaction | $\sigma_r$ (barns) |
|---|---|
| $^{27}Al$ (n,α) | 0.000705 |
| $^{58}Ni$ (n,p) | 0.1085 |
| $^{115}In$ (n,n′) | 0.189 |
| $^{238}U$ (n,f) | 0.308 |
| $^{237}Np$ (n,f) | 1.334 |

The appropriate measured reaction rates used for comparison with analytical prediction are summarized in Table 3.1.1-2.

In regard to the reaction rates listed in Table 3.1.1-2 it is important to note that, based on discussions contained in Reference 16, the $^{238}U$ and $^{237}Np$ data for locations within the pressure vessel wall (positions A4, A5, and A6) differ somewhat from the reaction rates given in References 3 and 17. In the earlier reports a 10% bias was noted between fission chamber measurements and solid state track recorder (SSTR) data. As a result, recommended reaction rates were taken to be the average of the two data sets. Since publication of those earlier documents, the observed bias was determined to be caused by perturbations in the neutron field caused by the presence of the fission chamber structure. Therefore, the SSTR measurements provided a more accurate representation of the $^{238}U$ (n,f) and $^{237}Np$ (n,f) reaction rates within the pressure vessel wall. The data listed in Table 3.1.1-2 incorporate only the SSTR results for positions A4, A5, and A6. Fission rate data for all other locations within the 12/13 configuration remain as reported in References 3 and 17.

In addition to the measured reaction rates for each of the individual neutron sensors, the documentation of the PCA experiments also provides recommended values for important energy dependent exposure parameters at each of the measurement locations. These derived exposure parameters resulting from the application of least squares adjustment procedures to fit an appropriate trial neutron energy spectrum

to each set of measured reaction rate data include $\phi(E > 1.0\ MeV)$, $\phi(E > 0.1\ MeV)$, and the iron atom displacement rate (dpa/sec). The recommended values of exposure parameters applicable to the 12/13 configuration are also listed in Table 3.1.1-2. The derived exposure parameters for locations A4, A5, and A6 reflect the use of $^{238}U$ and $^{237}Np$ fission rates measured by means of the SSTR technique. Thus, the influence of the previously mentioned bias associated with fission chamber perturbations has also been removed from these integral results.

The calculated reaction rates and exposure parameters applicable to the PCA 12/13 configuration and comparisons of these analytical predictions with the measurements are also provided in Table 3.1.1-2.

An examination of Table 3.1.1-2 shows that the calculated slope through the pressure vessel simulator shows a divergent trend relative to the measurements. This trend was also observed in prior analyses using ENDF/B-IV cross-sections. In an attempt to determine if currently observed trend is due to inadequacies in transport cross-sections or in the application of the two-dimensional synthesis technique to the analysis of a small reactor system, the PCA analysis was repeated using the TORT three-dimensional discrete ordinates transport code[14] in x,y,z geometry. The TORT analysis also used the BUGLE-93 cross-section library with a $P_3$ scattering cross-section expansion and an $S_8$ order of angular quadrature.

The results of the TORT three-dimensional calculations are provided in Table 3.1.1-3. Also provide in that table are the results of a least squares adjustment of the data supplied at each measurement location. An examination of Table 3.1.1-3 shows a remarkable improvement with the three-dimensional analysis. Also, agreement between the three-dimensional calculation and the best estimate exposure parameters obtained via the least squares adjustment is good with the calculated values tending to overpredict the best estimate at the inner surface of the pressure vessel simulator.

Table 3.1.1-2

Comparisons Of Measured And Calculated Data From The PCA Benchmark Evaluations

DORT Calculations

## Measured Data

| Location | Neutron Flux (E>1.0 ) | (E>0.1) | dpa/sec | $^{27}$Al (n,α) | $^{58}$Ni (n,p) | $^{115}$In (n,n') | $^{238}$U (n,f) | $^{237}$Np (n,f) |
|---|---|---|---|---|---|---|---|---|
| A0 | | | | | | | | |
| A1 | | | | 5.48E-09 | 6.31E-07 | 1.05E-06 | | |
| A2 | 4.01E-07 | 7.47E-07 | 5.85E-28 | 7.16E-10 | 6.72E-08 | 1.14E-07 | | 7.30E-07 |
| A3 | | | | 3.13E-10 | 2.50E-08 | 3.68E-08 | 5.91E-08 | 3.05E-07 |
| A4 | 4.50E-08 | 1.35E-07 | 7.41E-29 | 7.15E-11 | 5.69E-09 | 1.11E-08 | 1.79E-08 | 1.20E-07 |
| A5 | 2.21E-08 | 9.01E-08 | 4.20E-29 | 2.92E-11 | 2.25E-09 | 5.20E-09 | 7.88E-09 | 6.56E-08 |
| A6 | 9.73E-09 | 5.37E-08 | 2.22E-29 | 1.12E-11 | 7.99E-10 | 2.23E-09 | 3.26E-09 | 3.47E-08 |
| A7 | | | | 4.29E-12 | | 6.43E-10 | 8.65E-10 | 9.60E-09 |

## Absolute Calculation

| Location | Neutron Flux (E>1.0 ) | (E>0.1) | dpa/sec | $^{27}$Al (n,α) | $^{58}$Ni (n,p) | $^{115}$In (n,n') | $^{238}$U (n,f) | $^{237}$Np (n,f) |
|---|---|---|---|---|---|---|---|---|
| A0 | 1.60E-04 | 2.96E-04 | 2.22E-25 | 1.46E-07 | 2.23E-05 | 4.00E-05 | 6.71E-05 | 3.30E-04 |
| A1 | 3.76E-06 | 6.76E-06 | 5.66E-27 | 5.30E-09 | 6.05E-07 | 9.77E-07 | 1.68E-06 | 8.19E-06 |
| A2 | 4.18E-07 | 8.37E-07 | 6.37E-28 | 6.86E-10 | 6.47E-08 | 1.06E-07 | 1.80E-07 | 9.27E-07 |
| A3 | 1.38E-07 | 2.45E-07 | 2.12E-28 | 3.10E-10 | 2.46E-08 | 3.60E-08 | 6.28E-08 | 2.99E-07 |
| A4 | 4.54E-08 | 1.40E-07 | 7.48E-29 | 6.86E-11 | 5.48E-09 | 1.07E-08 | 1.72E-08 | 1.16E-07 |
| A5 | 2.13E-08 | 9.13E-08 | 4.11E-29 | 2.75E-11 | 2.14E-09 | 4.82E-09 | 7.39E-09 | 6.31E-08 |
| A6 | 9.15E-09 | 5.17E-08 | 2.07E-29 | 1.04E-11 | 7.89E-10 | 2.03E-09 | 2.95E-09 | 3.13E-08 |
| A7 | 2.16E-09 | 1.15E-08 | 4.69E-30 | 3.12E-12 | 1.96E-10 | 4.82E-10 | 6.95E-10 | 7.38E-09 |

## [M/C]

| Location | Neutron Flux (E>1.0 ) | (E>0.1) | dpa/sec | $^{27}$Al (n,α) | $^{58}$Ni (n,p) | $^{115}$In (n,n') | $^{238}$U (n,f) | $^{237}$Np (n,f) |
|---|---|---|---|---|---|---|---|---|
| A0 | | | | | | | | |
| A1 | | | | 1.03 | 1.04 | 1.08 | | |
| A2 | 0.96 | 0.89 | 0.92 | 1.04 | 1.04 | 1.08 | | 0.79 |
| A3 | | | | 1.01 | 1.02 | 1.02 | 0.94 | 1.02 |
| A4 | 0.99 | 0.96 | 0.99 | 1.04 | 1.04 | 1.04 | 1.04 | 1.04 |
| A5 | 1.04 | 0.99 | 1.02 | 1.06 | 1.05 | 1.08 | 1.07 | 1.04 |
| A6 | 1.06 | 1.04 | 1.07 | 1.08 | 1.01 | 1.10 | 1.11 | 1.11 |
| A7 | | | | 1.38 | | 1.33 | 1.24 | 1.30 |

Table 3.1.1-3
Comparisons Of Measured And Calculated Data From The PCA Benchmark Evaluations
TORT Calculations

Neutron Flux (E > 1.0 MeV)

| Location | Best Estimate | % Unc. | DORT | TORT | BE/DORT | BE/TORT |
|---|---|---|---|---|---|---|
| A1 | 3.87e-06 | 4 | 3.76e-06 | 3.83e-06 | 1.03 | 1.01 |
| A2 | 4.24e-07 | 4 | 4.18e-07 | 4.33e-07 | 1.01 | 0.98 |
| A3 | 1.37e-07 | 4 | 1.38e-07 | 1.44e-07 | 0.99 | 0.95 |
| A4 | 4.58e-08 | 4 | 4.54e-08 | 4.78e-08 | 1.01 | 0.96 |
| A5 | 2.23e-08 | 4 | 2.13e-08 | 2.24e-08 | 1.05 | 1.00 |
| A6 | 9.84e-09 | 5 | 9.15e-09 | 9.71e-09 | 1.08 | 1.01 |
| A7 | 2.79e-09 | 5 | 2.16e-09 | 2.62e-09 | 1.29 | 1.07 |

Iron Atom Displacement Rate (dpa)

| Location | Best Estimate | % Unc. | DORT | TORT | BE/DORT | BE/TORT |
|---|---|---|---|---|---|---|
| A1 | 5.84e-27 | 9 | 5.66e-27 | 5.64e-27 | 1.03 | 1.03 |
| A2 | 6.44e-28 | 8 | 6.37e-28 | 6.63e-28 | 1.01 | 0.97 |
| A3 | 2.14e-28 | 9 | 2.12e-28 | 2.21e-28 | 1.01 | 0.97 |
| A4 | 7.60e-29 | 6 | 7.48e-29 | 8.07e-29 | 1.02 | 0.94 |
| A5 | 4.41e-29 | 7 | 4.11e-29 | 4.47e-29 | 1.07 | 0.99 |
| A6 | 2.37e-29 | 8 | 2.07e-29 | 2.30e-29 | 1.14 | 1.03 |
| A7 | 6.72e-30 | 9 | 4.69e-30 | 6.33e-30 | 1.43 | 1.06 |

### 3.1.2 Comparisons with H.B. Robinson 2 Benchmark

At the onset of fuel Cycle 9, Carolina Power and Light Company entered into a cooperative venture with the NRC sponsored LWR Pressure Vessel Surveillance Dosimetry Improvement Program (LWR-PV-SDIP) and the Electric Power Research Institute (EPRI) to perform a series of measurements at the H. B. Robinson Unit 2 reactor. This multi-laboratory cooperative program included measurements both within the reactor cavity and within a replacement internal surveillance capsule attached to the thermal shield. The results of this program have been documented in reference 4 for use as a power reactor benchmark for testing analytical methodologies.

The analysis of the H. B. Robinson benchmark was carried out using the DORT two-dimensional $S_n$ transport code with the BUGLE-93 cross-section library. Dosimetry evaluations were also carried out using the least squares adjustment procedure described in Section 3.2. Results of the calculations and dosimetry evaluations are provided in Tables 3.1.2-1 through 3.1.2-3.

In Table 3.1.2-1, a comparison is provided of the measured and calculated reaction rates at both the internal surveillance capsule and the reactor cavity locations. The comparisons indicate good agreement at both locations with a slight trend toward overprediction by the calculation. The consistency of the agreement at the cavity and internal capsule locations indicates that the attenuation through the vessel wall is being calculated well by the ENDF/B-VI cross-sections. This observation matches that observed with the three-dimensional calculations performed for the PCA.

In Table 3.1.2-2, a comparison of the ratio of reaction rates at the surveillance capsule location to that at the cavity location is shown for each measured reaction. Data are provided for both calculation and measurement.

In Table 3.1.2-3, calculated exposure parameters in terms of $\phi(E > 1.0\ MeV)$ and dpa are provided along with the results of the least squares adjustment for both the internal capsule and the reactor cavity locations. Again, the trend toward overprediction by the calculation is evident. The results of the least squares evaluations show consistency with the reaction rate comparisons and the calculated and best estimate slopes are likewise in good agreement.

Table 3.1.2-1

Comparison of Measured and Calculated Reaction Rates
H.B. Robinson - Cycle 9 Benchmark

| | 20° Surveillance Capsule | | | 0° Reactor Cavity | | |
|---|---|---|---|---|---|---|
| Reaction | Calculated | Measured | M/C | Calculated | Measured | M/C |
| $^{63}Cu(n,\alpha)^{60}Co$ | 4.00e-17 | 3.98e-17 | 1.00 | 4.13e-19 | 4.01e-19 | 0.97 |
| $^{46}Ti(n,p)^{46}Sc$ | 6.35e-16 | 6.49e-16 | 1.02 | 5.92e-18 | 6.17e-18 | 1.04 |
| $^{54}Fe(n,p)^{54}Mn$ | 4.01e-15 | 3.83e-15 | 0.96 | 3.78e-17 | 3.59e-17 | 0.95 |
| $^{58}Ni(n,p)^{58}Co$ | 5.43e-15 | 4.88e-15 | 0.90 | 5.63e-17 | 5.29e-17 | 0.94 |
| $^{238}U(n,f)FP$ | 1.79e-14 | 1.80e-14 | 1.01 | 2.54e-16 | 2.72e-16 | 1.07 |
| $^{237}Np(n,f)FP$ | 1.24e-13 | 1.20e-13 | 0.97 | 5.23e-15 | | |
| Average | | | 0.97 | | | 0.99 |

Table 3.1.2-2

Comparison of Measured and Calculated Surveillance Capsule/Reactor Cavity Reaction Rates
H.B. Robinson - Cycle 9 Benchmark

| | Westinghouse Calculation | | | Measurement | | |
|---|---|---|---|---|---|---|
| Reaction | Capsule | Cavity | Ratio | Capsule | Cavity | Ratio |
| $^{63}Cu(n,\alpha)^{60}Co$ | 4.00e-17 | 4.13e-19 | 96.9 | 3.98e-17 | 4.01e-19 | 99.3 |
| $^{46}Ti(n,p)^{46}Sc$ | 6.35e-16 | 5.92e-18 | 107. | 6.49e-16 | 6.17e-18 | 105. |
| $^{54}Fe(n,p)^{54}Mn$ | 4.01e-15 | 3.78e-17 | 106. | 3.83e-15 | 3.59e-17 | 107. |
| $^{58}Ni(n,p)^{58}Co$ | 5.43e-15 | 5.63e-17 | 96.6 | 4.88e-15 | 5.29e-17 | 92.2 |
| $^{238}U(n,f)FP$ | 1.79e-14 | 2.54e-16 | 70.5 | 1.80e-14 | 2.72e-16 | 66.2 |
| $^{237}Np(n,f)FP$ | 1.24e-13 | 5.23e-15 | 23.7 | 1.20e-13 | | |

Table 3.1.2-3

Summary of Least Squares Evaluations
H.B. Robinson - Cycle 9 Benchmark

| | Calculated | Best Estimate | % Uncertainty | BE/C |
|---|---|---|---|---|
| | | 20° Surveillance Capsule | | |
| $\phi(E > 1.0$ MeV) | 4.89e+10 | 4.58e+10 | 7 | 0.94 |
| dpa/sec | 7.75e-11 | 7.36e-11 | 9 | 0.95 |
| Avg. Foil M/C | | | | 0.97 |
| | | 0° Reactor Cavity | | |
| $\phi(E > 1.0$ MeV) | 9.78e+08 | 9.54e+08 | 10 | 0.98 |
| dpa/sec | 4.16e-12 | 4.11e-12 | 20 | 0.99 |
| Avg. Foil M/C | | | | 0.99 |
| | | Surveillance Capsule/Cavity Ratio | | |
| $\phi(E > 1.0$ MeV) | 50.0 | 48.0 | | 0.96 |
| dpa/sec | 18.6 | 17.9 | | 0.96 |

## *3.2 Dosimetry Methodology Comparisons*

### 3.2.1 General Description of Adjustment Methods

Adjustment methods provide the capability of combining the measurement data with the neutron transport calculation resulting in a best estimate spectrum and exposure parameters with associated uncertainties. The use of measurements in combination with the analytical results reduces the uncertainties and acts to remove biases present in the analytical technique. In general, the adjustment methods, as applied to reactor vessel fluence evaluations, act to reconcile the reaction rate data, dosimeter cross-sections, and input spectrum within the given uncertainties. For example,

$$R_i \pm \delta_{R_i} = \sum_g (\sigma_{ig} \pm \delta_{\sigma_{ig}})(\phi_g \pm \delta_{\phi_g})$$

Eq. 3.2-1

relates a set of measure reaction rates $R_i$ to a single spectrum $\phi_g$ by the multigroup reaction cross-section $\sigma_{ig}$, each with an uncertainty denoted by $\delta$.

The use of adjustment methods in neutron fluence analysis is not new. ASTM has addressed the use of adjustment methods in ASTM E944 Standard and many industry workshops have been held to discuss the various methods. For example, the ASTM-EURATOM Symposia on Reactor Dosimetry hold workshops on neutron spectrum unfolding and adjustment techniques at each of the conferences.

ASTM E944 Standard

The use of an adjustment procedure to evaluate the best estimate neutron exposure parameters and their uncertainties from Light Water Reactors is described in ASTM E944 Standard. Specifically, paragraph 3.3.2.1 of E944 states:

*"The algorithms of the adjustment codes tend to decrease the variances of the adjusted data compared to the corresponding input values. The least squares adjustment codes yield estimates for the output data with minimum variances, that is, the 'best' estimates. This is the primary reason for using these adjustment procedures."*

The primary objective of the adjustment code is to produce unbiased estimates of the neutron exposure parameters. The analytical method alone is deficient because it inherently contains biases due to the input assumptions, such as the temperature of the water in the peripheral assemblies, by-pass region, and down-comer regions, component dimensions, and peripheral core source. Due to the relatively large uncertainty (±20%) associated with the calculations, accurate dosimetry measurements must be obtained from sensor sets that respond to a variety of regions of the neutron energy spectrum.

The Palisades dosimetry set conform with the ASTM E844 Standard[18] for sensor set design and irradiation and adequately covers the neutron energy spectrum and provides overlap as shown in Table 3.2.1-1.

Table 3.2.1-1
Palisades Neutron Dosimetry Set

| Monitor Material | Reaction of Interest | Detector Response | Product Half-life |
|---|---|---|---|
| Copper | $^{63}Co$ (n,α) $^{60}Co$ | E > 4.7 MeV | 5.271 y |
| Titanium | $^{46}Ti$ (n,p) $^{46}Sc$ | E > 4.4 MeV | 83.83 d |
| Iron | $^{54}Fe$ (n,p) $^{54}Mn$ | E > 1.0 MeV | 312.5 d |
| Nickel | $^{58}Ni$ (n,p) $^{58}Co$ | E > 1.0 MeV | 70.78 d |
| Uraniun-238 | $^{238}U$ (n,f) $^{137}Cs$ | E > 0.4 MeV | 30.17 y |
| Neptunium-237 | $^{237}Np$ (n,f) $^{137}Cs$ | E > 0.08 MeV | 30.17 y |
| Cobalt-Aluminum | $^{59}Co$ (n,γ) $^{60}Co$ | E > 0.015 MeV | 5.271 y |

Summary of Available Adjustment Codes

ASTM E944 Standard provides a listing of available adjustment codes. A few of the more common codes employed in reactor surveillance programs are STAY'SL[19], LSL-M2[20], LEPRICON[21], and FERRET[12,22]. Each of these codes is publicly available from RSICC at ORNL. The information provided for STAY'SL, LSL-M2, and LEPRICON is taken directly from the code abstracts published by RSICC at ORNL.

STAY'SL is a least-squares fitting code system which solves the dosimetry unfolding problem and provides a statement of the uncertainties in the group fluxes due to the uncertainties in the activation data, dosimetry cross sections, and input group fluxes.

STAY'SL does not solve the usual dosimetry unfolding problem in the sense that it provides a statement of the most likely joint probability density function of the group fluxes, i.e., the spectrum, given the joint probability density function of some measured activation, dosimetry cross sections, and some a priori input group fluxes. The density functions are assumed to be normal and independent for the three classes of input data. The joint probability density functions of each class of input data except for being normal may be completely arbitrary. With the above restrictions on the density functions of the input data, STAY'SL may be thought of as performing the complete "error analysis" in the solution to the dosimetry unfolding problem.

STAY'SL uses the least-squares method to obtain its solution. Because the three different types of input data are assumed to have independent probability density functions, in particular the activation data, the method of solution is extremely fast and requires only the inversion of a small matrix of dimensions equal to the number of activation measurements. This matrix will very seldom be singular; therefore, a solution may almost always be obtained.

Although the method is also formally equivalent to a "dosimetry cross section adjustment," STAY'SL does not solve for the "adjusted cross sections". The joint probability density function of the output group fluxes, which is the solution, reflects the uncertainties in the input dosimetry cross sections as given by their input joint probability density function.

Because the activation data are assumed to have a probability density function, independent of the other input data, the method is equivalent to an application of Bayes' theorem where the activation data are used to improve upon some a priori knowledge of the distribution of the spectrum for which a solution is needed, given an a priori distribution of the dosimetry cross sections.

LSL-M2 adjusts calculated neutron spectra to make the fluence values consistent with given neutron dosimetry measurements. The primary output is a set of values for the best estimates of damage parameter values; the solution is based on a least squares fit of all input data.

In an adjustment procedure, consistency is achieved by adjusting the input data in such a manner that a weighted sum of squares of adjustments is minimized. The weights are assigned according to the input uncertainties, i.e., the larger the uncertainty, the smaller the weight. This sum, which is further modified by correlations, represents the negative logarithm of the probability of the outcome of the experiment if the adjusted values are the "true" data.

The LEPRICON system provides state-of-the-art routines to prepare input for and process results from the discrete ordinates codes to determine best estimates with uncertainties of group fluences in pressure vessels of pressurized water reactors. The system anticipates availability of results of dosimetry measurements performed in the reactor as well as sources operating during the time of exposure.

Effects of time-dependent core source spatial distributions, when necessary, are treated by the use of an adjoint function coupled with a scaling technique. Sources are generated by combining the results of the diffusion theory code pin-wise calculations with in-core assembly-wise instrumentation and are converted from X-Y to R-Θ geometry. Fluxes calculated by the discrete ordinates codes are then synthesized to form 3-D distributions, and the resulting calculated dosimeter responses compared with the measurements, and adjustments performed in a generalized linear least-squares combination procedure. Through correlations generated from the input, adjustments to the originally calculated group fluxes at a selected point in the pressure vessel are then made, and the best estimates of the fluences accumulated during the time period analyzed are output along with their reduced uncertainties.

Westinghouse employs the FERRET code to perform the least squares analysis of the neutron exposure for the reactor surveillance dosimetry, both in-vessel and ex-vessel. The FERRET code was developed at the Hanford Engineering Development Laboratory and used in the characterization of the Fast Test Reactor (FTR)[23].

In the FERRET code, a log-normal least squares algorithm weights both the calculated or trial values and the measured data in accordance with the assigned uncertainties and correlations. In general, the measured values $f$ are linearly related to the flux $\phi$ by some response matrix $A$:

$$f_i^{(s,\alpha)} = \sum_g A_{ig}^{(s)} \phi_g^{(\alpha)} \qquad \text{Eq. 3.2-2}$$

where $i$ indexes the measured values belonging to a single data set $s$, $g$ designates the energy group,

and $\alpha$ delineates spectra that may be simultaneously adjusted. The log-normal approach automatically accounts for the physical constraint of positive fluxes, even with large assigned uncertainties.

### 3.2.2 Testing and Application of the FERRET Least Squares Analysis

General Description of the Adjustment Procedure

The FERRET code was initially developed at the Hanford Engineering Development Laboratory in Richland, Washington and is available to the general public through the Radiation Shielding Information Center (RSIC) at the Oak Ridge National Laboratory as Computer Code Package PRS-145. The FERRET least squares adjustment approach has had extensive use in both the Liquid Metal Fast Breeder (LMFBR) program and the NRC sponsored Light Water Reactor Dosimetry Improvement Program (LWR-PV-SDIP).

As a result of participation in several cooperative efforts associated with the LWR-PV-SDIP, the FERRET approach was adopted by Westinghouse in the mid 1980's as the preferred approach for the evaluation of LWR surveillance dosimetry. The least squares adjustment methodology was judged superior to the spectrum averaged cross-section approach that is totally dependent on the accuracy of the calculated neutron spectrum at the measurement locations.

The FERRET code is currently employed to combine the results of plant specific neutron transport calculations and multiple foil reaction rate measurements to determine best estimate values of exposure parameters ($\phi$(E > 1.0 MeV) and dpa) along with associated uncertainties at both in-vessel and ex-vessel measurement locations.

The application of the least squares methodology requires the following input:

1. The calculated neutron energy spectrum and associated uncertainties at the measurement location.
2. The measured reaction rate and associated uncertainty for each sensor contained in the multiple foil set.
3. The energy dependent dosimetry reaction cross-sections and associated uncertainties for each sensor contained in the multiple foil set.

For a given application, the calculated neutron spectrum is obtained from the results of plant specific neutron transport calculations applicable to the irradiation period experienced by the dosimetry sensor set. This calculation is performed using the benchmarked calculational methodology described earlier in this report. The sensor reaction rates are derived from measured specific activities obtained from the counting laboratory using the specific irradiation history of the sensor set to perform decay corrections. The dosimetry reaction cross-sections and uncertainties are obtained from the SNLRML dosimetry cross-section library. There are no additional data or data libraries built into the FERRET code system. All of the required input is supplied externally at the time of the analysis.

The overall least squares evaluation of a given data set can be conveniently divided into two steps;

a pre-adjustment procedure performed by the SAND module that processes the calculated spectrum and dosimetry cross-sections into the 53 energy group structure required by FERRET and the subsequent application of the least squares algorithm in the FERRET module itself. The steps in the pre-adjustment processing can be summarized by the following steps:

1. The calculated neutron energy spectrum in the BUGLE-93 47 energy group structure is input to the SAND module.
2. The input spectrum is expanded to 620 energy groups to provide compatibility with the SNLRML dosimetry cross-section library.
3. The 620 group neutron spectrum is combined with the dosimetry cross-section library to compute spectrum weighted cross-sections in the 53 energy group structure used in the FERRET module.
4. The 620 group spectrum is likewise collapsed to the 53 energy group structure used in FERRET.

The application of this pre-processing procedure allows the fine group dosimetry cross-sections to be spectrally weighted by a calculated spectrum representative of the actual measurement location in the reactor. This approach, if executed properly, is superior to the use of broad group dosimetry cross-sections that have been collapsed with an arbitrary spectrum. Broad group dosimetry cross-sections weighted over a "flat" spectrum and a "Pressure Vessel ¼T" spectrum are supplied with the BUGLE-93 library.

The second step in the FERRET least squares adjustment procedure may be summarized as follows:

1. The 53 group neutron energy group spectrum and dosimetry reaction cross-sections output from the SAND module are input to the FERRET module along with the measured reaction rate for each sensor included in the multiple foil sensor set. It should be noted that this input includes uncertainty estimates for the neutron spectrum, cross-sections, and reaction rates.
2. The least squares evaluation of the input data is performed by the FERRET module.
3. Best Estimates of neutron exposure parameters ($\phi$(E > 1.0 MeV) and dpa) along with associated uncertainties are output by the FERRET module.

It is important to note that the least squares adjustment performed by the FERRET code is limited to the data evaluation at the measurement location. The purpose of this stage of the overall evaluation is to obtain best estimates of the neutron exposure at the measurement location in terms of $\phi$(E > 1.0 MeV) and dpa as well as to estimate the uncertainty associated with these exposure parameters. The FERRET code DOES NOT perform an adjustment of the neutron spectrum at the pressure vessel wall.

Testing of the FERRET Procedure in the $^{235}$U Thermal Fission Field

In ASTM E 261 - 96, "Standard Practice for Determining Neutron Fluence Rate, Fluence, and Spectra by Radioactivation Techniques,"[24] fission spectrum averaged cross-sections applicable to the $^{235}$U thermal fission field are provided for threshold activation detectors that are typically used in power and research reactor irradiations. In this data compilation, both calculated and measured spectrum averaged cross-sections are provided along with their uncertainties. The following data have been extracted from Table 3 of ASTM

E 261 - 96 as representative of the foil sets typically used in power reactor irradiations as well as of those used in the PCA benchmark irradiations:

Table 3.2.2-1

$^{235}U$ Fission Spectrum Averaged Cross-Sections for Power Reactor Sensor Sets

| Reaction | Calculation (mb)[a] | Measured (mb)[b] | C/E[c] |
|---|---|---|---|
| $^{63}Cu$ (n,α) $^{60}Co$ | 0.521 (2.85%,6.05%) | 0.50 (11%) | 1.042 (12.87%) |
| $^{46}Ti$ (n,p) $^{46}Sc$ | 10.43 (2.46%,5.40%) | 11.6 (3.45% | 0.899 (6.86%) |
| $^{54}Fe$ (n,p) $^{54}Mn$ | 80.18 (2.17%,4.69%) | 80.5 (2.86%) | 0.996 (5.91%) |
| $^{58}Ni$ (n,p) $^{58}Co$ | 105.69 (2.43%,4.52%) | 108.5 (5.0%) | 0.974 (7.16%) |
| $^{238}U$ (n,f) FP | 306.23 (0.53%,4.21%) | 309.0 (2.6%) | 0.991 (4.98%) |
| $^{237}Np$ (n,f) FP | 1330.1 (9.33%,4.31%) | 1344.0 (4.0%) | 0.990 (4.98%) |

Table 3.2.2-2

$^{235}U$ Fission Spectrum Averaged Cross-Sections for PCA Sensor Sets

| Reaction | Calculation (mb)[a] | Measured (mb)[b] | C/E[c] |
|---|---|---|---|
| $^{27}Al$ (n,α) $^{24}Na$ | 0.727 (1.40%,6.95%) | 0.706 (3.97%) | 1.030 (8.13%) |
| $^{58}Ni$ (n,p) $^{58}Co$ | 105.69 (2.43%,4.52%) | 108.5 (5.0% | 0.974 (7.16%) |
| $^{115}In$ (n,n') $^{115m}In$ | 186.35 (2.17%,4.17%) | 190.3 (3.84%) | 0.979 (6.07%) |
| $^{103}Rh$ (n,n') $^{103m}Rh$ | 706.02 (3.1%, 4.14%) | 733.0 (5.2%) | 0.963 (7.33%) |
| $^{238}U$ (n,f) FP | 306.23 (0.53%,4.21%) | 309.0 (2.6%) | 0.991 (4.98%) |
| $^{237}Np$ (n,f) FP | 1330.1 (9.33%,4.31%) | 1344.0 (4.0%) | 0.990 (4.98%) |

Notes for Tables 3.2.2-1 and 3.2.2-2:

a) The cross-section and spectrum components of uncertainty, respectively, are in parentheses.
b) The measurement uncertainty appears in parentheses.
c) The uncertainty represents a sum in quadrature of the measurement and calculational uncertainty.

In order to test the pre-processing procedure used in the SAND module to expand the calculated input spectrum, spectrum weight the dosimetry cross-sections, and re-collapse the spectrum and dosimetry cross-sections to the FERRET 53 energy group structure, FERRET runs were performed for the sensor sets listed in Tables 3.2.2-1 and 3.2.2-2. In performing these FERRET runs, the ENDF/B-VI $^{235}U$ fission spectrum supplied with the BUGLE-93 library was input as the calculated spectrum and the measured spectrum averaged cross-sections were input as the measured reaction rates. Dosimetry reaction cross-sections were obtained directly from the SNLRML library.

Comparisons of the FERRET calculated spectrum averaged cross-sections prior to

adjustment with the calculated values from ASTM E 261-96 are provided in Tables 3.2.2-3 and 3.2.2-4 for the power reactor and PCA sensor sets, respectively. An examination of Tables 3.2.2-3 and 3.2.2-4 shows that the spectrum averaged cross-sections calculated by the SAND pre-processing module are in excellent agreement with the calculated values provided in ASTM E 261-96 with the largest difference being at the 1% level.

This comparison demonstrates that using the SNLRML dosimetry cross-section library along with the algorithms employed in the SAND pre-processing module to expand the calculated neutron spectrum, weight the dosimetry cross-sections, and re-collapse both spectrum and cross-sections to the FERRET group structure results in an appropriate spectrum and cross-section representation for use in the least squares adjustment algorithm. That is, the pre-processing procedure DOES NOT introduce distortions in either the input spectrum or the input dosimetry reaction cross-sections.

Table 3.2.2-3

$^{235}U$ Fission Spectrum Averaged Cross-Sections for Power Reactor Sensor Sets

| Reaction | ASTM E 261 - 96 Calculation (mb) | FERRET Calculation (mb) | Ratio FERRET/E 261 |
|---|---|---|---|
| $^{63}Cu$ (n,α) $^{60}Co$ | 0.521 | 0.523 | 1.004 |
| $^{46}Ti$ (n,p) $^{46}Sc$ | 10.4 | 10.3 | 0.990 |
| $^{54}Fe$ (n,p) $^{54}Mn$ | 80.2 | 80.3 | 1.001 |
| $^{58}Ni$ (n,p) $^{58}Co$ | 106 | 106 | 1.000 |
| $^{238}U$ (n,f) FP | 306 | 306 | 1.000 |
| $^{237}Np$ (n,f) FP | 1330 | 1330 | 1.000 |

Table 3.2.2-4

$^{235}U$ Fission Spectrum Averaged Cross-Sections for PCA Sensor Sets

| Reaction | ASTM E 261 - 96 Calculation (mb) | FERRET Calculation (mb) | Ratio FERRET/E 261 |
|---|---|---|---|
| $^{27}Al$ (n,α) $^{24}Na$ | 0.727 | 0.729 | 1.003 |
| $^{58}Ni$ (n,p) $^{58}Co$ | 106 | 106 | 1.000 |
| $^{115}In$ (n,n') $^{115m}In$ | 186 | 186 | 1.000 |
| $^{103}Rh$ (n,n') $^{103m}Rh$ | 706 | 706 | 1.000 |
| $^{238}U$ (n,f) FP | 306 | 306 | 1.000 |
| $^{237}Np$ (n,f) FP | 1330 | 1330 | 1.000 |

# 4.0 Analytical Sensitivity Studies

The overall uncertainty associated with calculated exposure rates and integrated exposures can be conveniently subdivided into two broad categories. The first category involves biases or errors that may be present due to inadequacies in the method itself or in the basic nuclear data input to the calculation. These potential biases are addressed via validation of the analytical technique through comparison with measurements from controlled benchmark experiments, from power reactor surveillance capsule and reactor cavity measurement data bases, and, ultimately, from plant specific surveillance capsule and cavity irradiations. The use of these analytical/measurement comparisons to effectively remove potential biases from analytical predictions results in best estimate projections of vessel exposure.

The second category of uncertainty in the analysis of vessel exposure involves variations that may exist in reactor dimensions, coolant temperature, neutron source strength and source distribution, as well as in other parameters that may vary from reactor to reactor or fuel cycle to fuel cycle. This category of uncertainty is most easily addressed via sensitivity studies performed for each of the variables important to the overall evaluation.

For the methodology used in the light water reactor neutron exposure evaluations, several sensitivity studies were carried out to test the effect of variations in reactor geometry and neutron source definition on the calculated vessel exposure based on the analytical approach. These studies are not all inclusive, but do encompass the major contributors to uncertainties in the analytical approach. Important input parameters addressed in these studies include the following:

Geometry and Material Density
- stainless steel reactor internals
- water annuli
- reactor pressure vessel
- core periphery modeling
- dosimetry positioning (capsule/cavity)

Core Neutron Source
- peripheral assembly source magnitude
- peripheral assembly burnup
- axial power distribution
- relative spatial distribution of the source

As noted earlier, the effects of transport cross-section errors and uncertainties as well as biases introduced by methods approximations were obtained by direct comparisons with measured data rather than via a series of analytical studies.

## 4.1 Geometric Modeling and Material Density

The calculations performed for the Palisades reactor made use of nominal design dimensions for the internals components to establish the reactor geometry used in the transport model. For the reactor vessel inner radius, as-built data was available and reactor vessel thickness measurements made with an ISI tool was also available. Both were incorporated into the model. Likewise, the average core and vessel inlet coolant temperatures were used to determine water density in the core, bypass and downcomer regions. Sensitivity of the calculated fast neutron exposure of the pressure vessel to each of these variables was addressed via a series of parametric studies documented in WCAP-13390[25] which was included as part of a 1992 submittal regarding the Palisades vessel fluence.

To determine the potential impact of the reactor internals manufacturing and assembly tolerances on the analytical prediction of the fast neutron exposure of the pressure vessel, calculations were performed for cases representing minimum shielding between the reactor core and the pressure vessel (i.e., all components at minimum thickness) and for maximum shielding between the core and the pressure vessel (i.e., all components at maximum thickness). These extreme conditions were then compared to the nominal calculation to establish an upper bound uncertainty in the use of nominal vs as-built internals dimensions. The resultant uncertainty in the calculated exposure of the pressure vessel is ±3%.

The sensitivity of the calculated vessel exposure to fluctuations in water temperature are likewise determined via a parametric study in which water temperature and, hence, coolant density is varied over a range of several degrees F relative to nominal conditions. The results of this study indicate that a bounding uncertainty of ±4% results from a temperature variation of ±10°F. A ±10° fluctuation in water temperature would exceed variations expected during normal operation of the plant over a given fuel cycle. Thus, the projected 4% uncertainty is considered to represent a conservative upper bound estimate.

The modeling of the rectilinear core baffle in r,θ geometry represents another potential source of uncertainty in the geometric modeling of the reactor. The sensitivity of the solution to the modeling approach was determined by a direct comparison of the results of an r,θ computation with those of an x,y calculation in which the baffle region and core periphery were modeled explicitly. The comparisons of interest were taken at various locations external to the core baffle. Results of these calculations, in general agreed within the pointwise flux convergence criterion specified for the transport analyses, thus, demonstrating the adequacy of the modeling approach. Therefore, the bounding analytical uncertainty associated with this modeling approximation is taken to be less than ±1%.

It should be noted that the x,y vs r,θ comparisons described in the preceding paragraph, address not only the adequacy of the geometric modeling of the core periphery, but, also demonstrate the adequacy of the transformation of the core neutron source from pin powers to the r,θ DORT model.

The inner radius of the reactor vessel itself and the position of surveillance capsule dosimetry are extremely important in the determination of the exposure of the pressure vessel wall both from an analytical standpoint and from the viewpoint of surveillance capsule and reactor cavity dosimetry interpretation. Therefore, sensitivity studies based on the dimensions for both the vessel inner radius and capsule position are also performed.

Parametric evaluations of vessel inner radius indicate that variations in vessel inner radius result in a change in calculated vessel fast neutron exposure of ±5%. Uncertainties associated with the positioning of capsule dosimetry are extremely important in the evaluation of comparisons of calculation with measurement and the subsequent determination of plant specific bias factors. Parameter studies using the dimensional variations result in positioning uncertainties of ±4% for surveillance capsules.

In developing the above uncertainties, the parametric studies are based on the assumption that, in the case of the surveillance dosimetry, displacement of the sensors either introduced or removed water from the area between the reactor core and the sensors.

## *4.2 Core Neutron Source*

In addition to the sensitivity of the transport calculation to tolerances in the geometric model, several studies were also carried out to establish the sensitivity to the strength and spatial distribution of the neutron source within the reactor core. In particular, investigations were carried out to determine the sensitivity of calculated results to the absolute source strength in fuel assemblies on the core periphery, the pin by pin spatial distribution of neutron source on the core periphery, the burnup of peripheral fuel assemblies, and the axial power distribution used in the flux synthesis procedure. It should be noted that the impacts of changing fission spectra, energy release per fission, and neutron yield per fission were encompassed in the parametric variation of fuel assembly burnup.

In regard to the absolute power level of peripheral fuel assemblies, the self-attenuation afforded by the core materials results in the neutron environment external to the core being dominated by these edge assemblies. An examination of the adjoint transport evaluations performed for a typical reactor geometry demonstrates that 90-95% of the external environment results from neutrons born in these locations. Therefore, the fluence uncertainty associated with the absolute core power level is directly dependent on the uncertainties in the power production of those peripheral assemblies. Based on comparisons of calculated vs measured (derived from in-core flux maps) peripheral power distributions for pressurized water reactors an uncertainty for peripheral power magnitude has been determined to be on the order of ±5% relative to an assembly power of 1.0. Additional uncertainty in vessel exposure calculations is introduced by the power distribution gradient across the peripheral fuel assemblies. These additional uncertainties are difficult to determine, however, use of the dosimetry measurements in determining the best estimate fluence accounts for these.

In a fashion similar to the peripheral assembly power, the uncertainty in the axial power distribution averaged over the irradiation period, translates directly to an uncertainty in the calculated

neutron environment external to the core. Over the course of a given fuel cycle, the variation in the axial peaking factor at maximum flux locations is typically 10%. That is, the maximum axial peaking factor may change from a value of approximately 1.15 at beginning of cycle to 1.05 at end of cycle, yielding a cycle average peaking factor of 1.10. This observation is drawn from an examination of numerous axial distributions from a wide variety of pressurized water reactors employing both low leakage and non-low leakage fuel management. In order to bound the uncertainty associated with this cycle average value, a variation of ±5% is taken to be applicable. This uncertainty value is liberal enough to encompass the entire change in axial shape over the course of the fuel cycle.

Sensitivity studies involving source parameters such as fission spectrum, neutron yield per fission and energy release per fission were performed via an evaluation of the sensitivity of the calculated fast neutron flux at the pressure vessel inner radius to the burnup of assemblies on the periphery of the reactor core. These burnup studies encompass significant perturbations in these source parameters due to the build-in of plutonium isotopes as the assembly burnup increases.

For the studies in question, burnup was varied from an assembly average of 3,000 MWD/MTU to 45,000 MWD/MTU. The results of this evaluation indicated that the net change in vessel flux is approximately +0.4% per 1,000 MWD/MTU in the burnup range of 3,000-15,000 MWD/MTU and +0.2% per 1,000 MWD/MTU in the burnup range of 15,000-45,000 MWD/MTU. The total increase in calculated flux at a burnup of 45,000 MWD/MTU relative to that based on a burnup of 3,000 MWD/MTU is about 10%.

The values quoted in the preceding paragraph are typical of light water reactors. Actual values will vary slightly depending on reactor core configuration, core loading, and the location of the point of interest on the vessel wall. However, these smaller changes are of second order and, therefore, the data discussed above provide an adequate evaluation of the sensitivity of the neutron flux at the pressure vessel and at dosimetry locations to these particular parameters.

In the assignment of an overall sensitivity to fuel assembly burnup a liberal approach is utilized. It is first assumed that the sensitivity to burnup effects was +0.4% per 1,000 MWD/MTU; i.e., the largest value obtained from the sensitivity study. It is then further assumed that from the plant specific core design information, a 5,000 MWD/MTU uncertainty exists in the calculated fuel assembly burnup. This is clearly a conservative evaluation, particularly at low to intermediate levels of burnup. Combining these two values yields a bounding sensitivity to fission spectrum, neutron yield per fission, and energy release per fission of ±2%.

## *4.3 Summary of Analytical Sensitivity Studies*

The results of analytically based sensitivity studies of geometric and source distribution input parameters may be summarized in Table 4.3-1.

When combined these individual sensitivities result in a net impact on the calculated flux levels in the vicinity of the pressure vessel of ±11%. The uncertainty evaluated at the dosimeter

locations within internal surveillance capsules is ±10%.

These uncertainties due to potential variations in design and operating parameters for individual reactors must, of course be combined with biases resulting from methods and cross-section errors to determine the total uncertainty in the calculated results.

Table 4.3-1
Summary of Analytical Sensitivities

| | Vessel IR | Capsule |
|---|---|---|
| r,θ Modeling | 1% | 1% |
| Internals Dimensions | 3% | 3% |
| Vessel Inner Radius | 5% | |
| Water Temperature | 4% | 3% |
| Peripheral Assembly Source Strength | 5% | 5% |
| Axial Power Distribution | 5% | 5% |
| Peripheral Assembly Burnup | 2% | 2% |
| Spatial Distribution of the Source | 4% | 4% |
| Capsule Dosimetry Positioning | | 4% |
| TOTAL $[\Sigma \sigma_i]^{0.5}$ | 11% | 10% |

# 5.0 References


1. 10 CFR 50.61, "Fracture Toughness Requirements for Protection Against Pressurized Thermal Shock Events".
2. Draft Regulatory Guide DG-1053, "Calculational and Dosimetry methods for Determining Pressure Vessel Neutron Fluence," U.S. Nuclear Regulatory Commission, Office of Nuclear Regulatory Research, September 1993.
3. Remec, I. and Kam, F. B. K., "Pool Critical Assembly Pressure Vessel Facility Benchmark," NUREG/CR-6454, Nuclear Regulatory Commission, Washington, D. C., July 1996.
4. Remec, I. and Kam, F. B. K., "H. B. Robinson-2 Pressure Vessel Benchmark," NUREG/CR-6453, Nuclear Regulatory Commission, Washington, D. C., October 1997.
5. Andrachek, J. D., et al., "Methodology Used to Develop Cold Overpressure Mitigating System Setpoints and RCS Heatup and Cooldown Limit Curves," WCAP-14040-NP-A, January 1996.
6. Bohl, Jr., H., et al., "P1MG - A One Dimensional Multigroup $P_1$ Code for the IBM-704,: WAPD-TM-135, July 1959.
7. Soltesz, R. G., Disney, R. K., "Nuclear Rocket Shielding Methods, Modification, Updating and Input Data Preparation - Volume 4 - One-Dimensional Discrete Ordinates Transport Technique," WANL-PR-(LL)-034, August 1970
8. Soltesz, R. G., et al.., "Nuclear Rocket Shielding Methods, Modification, Updating and Input Data Preparation - Volume 5 - Two-Dimensional Discrete Ordinates Transport Technique," WANL-PR-(LL)-034, August 1970.
9. Soltesz, R. G., et al.., "Nuclear Rocket Shielding Methods, Modification, Updating and Input Data Preparation - Volume 2 - Compilation of Neutron and Photon Cross Section Data," WANL-PR-(LL)-034, August 1970.
10. Anderson, S. L., "Characterization of the Neutron Environment for Commercial LWR Pressure Vessel Surveillance Programs," Proceeding of the Second ASTM-EURATOM Symposium on Reactor Dosimetry, NUREG/CP-0004, Vol. 3, pp. 1093-1107, October 3-7, 1977.
11. RSIC Data Library Collection DLC-76, SAILOR, "Coupled, Self-Shielded, 47 Neutron, 20 Gamma-Ray, $P_3$, Cross-Section Library for Light Water Reactors," March 1983.
12. FERRET, "Least-Squares Solution to Nuclear Data and Reactor Physics Problems," RSIC Code Package PSR-145, Oak Ridge National Laboratory, March 1984.
13. ASTM Designation E944-96, "Standard Guide for Application of Neutron Spectrum Adjustment Methods in Reactor Surveillance," in ASTM Standards, Section 12, American Society for Testing and Materials, Philadelphia, PA, 1997.
14. RSIC Computer Code Collection CCC-543, "TORT-DORT Two- and Three-Dimensional Discrete Ordinates Transport, Version 2.7.3", May 1993.
15. RSIC Data Library Collection DLC-175, "BUGLE-93, Production and Testing of the VITAMIN-B6 Fine Group and the BUGLE-93 Broad Group Neutron/Photon Cross-Section Libraries Derived from ENDF/B-VI Nuclear Data", April 1994.
16. McElroy, W. N., et al., "LWR Pressure Vessel Surveillance Dosimetry Improvement Program: PCA Experiments and Blind Test," NUREG/CR-1861, Nuclear Regulatory Commission, Washington, D.C., July 1981.

17. McElroy, W. N., et al., "LWR Pressure Vessel Surveillance Dosimetry Improvement Program: PCA Experiments, Blind Test, and Physics-Dosimetry Support for the PSF Experiments," NUREG/CR-3318, Nuclear Regulatory Commission, Washington, D.C., September 1984.
18. ASTM Designation E844-86 (Re-approved 1991), "Standard Guide for Sensor Set Design and Irradiation for Reactor Surveillance," in ASTM Standards, Section 12, American Society for Testing and Materials, Philadelphia, PA, 1997.
19. STAY'SL, "Least Squares Dosimetry Unfolding Code System," RSIC Code Package PSR-113, Oak Ridge National Laboratory, December 1991.
20. LSL-M2, "Least-Squares Logarithmic Adjustment of Neutron Spectra," RSIC Code Package PSR-233, Oak Ridge National Laboratory, February 1991.
21. LEPRICON, "PWR Pressure Vessel Surveillance Dosimetry Analysis System," RSIC Code Package PSR-277, Oak Ridge National Laboratory, June 1995.
22. A. Schmittroth, "FERRET Data Analysis Code", HEDL-TME 79-40, Hanford Engineering Development Laboratory, Richland, WA, September 1979.
23. Lippincott, E. P., McElroy, W. N., "FTR Dosimetry Handbook," HEDL MG-166, Hanford Engineering Development Laboratory, March 1983.
24. ASTM Designation E261-96, "Standard Practice for Determining Neutron Fluence Rate, Fluence, and Spectra by Radioactivation Techniques," in ASTM Standards, Section 12, American Society for Testing and Materials, Philadelphia, PA, 1997.
25. S.L. Anderson, "Westinghouse Fast Neutron Exposure Methodology for Pressure Vessel Fluence Determination and Dosimetry Evaluation," WCAP-13390, May 1992.